J Eng Math (2007) 59:123–137
DOI 10.1007/s10665-006-9084-8

ORIGINAL ARTICLE

Effect of pulsations on two-layer channel flow

M. G. Blyth

Received: 14 March 2006 / Accepted: 13 July 2006 / Published online: 11 October 2006

Abstract The effect of vertical wall vibrations on two-phase channel flow is examined. The basic flow consists of two superposed fluid layers in a channel whose walls oscillate perpendicular to themselves in a prescribed, time-periodic manner. The solution for the basic flow is presented in closed form for Stokes flow, and its stability to small periodic perturbations is assessed by means of a Floquet analysis. It is found that the pulsations have a generally destabilizing influence on the flow. They tend to worsen the Rayleigh–Taylor instability present for unstably stratified fluids; the larger the amplitude of the pulsations, the greater the range of unstable wave numbers. For stably stratified fluids, the pulsations raise the growth rate of small perturbations, but are not sufficient to destabilize the flow. In the latter part of the paper, the basic flow for arbitrary Reynolds number is computed numerically assuming a flat interface, and the motion of the interface in time is predicted. The existence of a time-periodic flow is demonstrated in which the ratio of the layer thicknesses remains constant throughout the motion.

Keywords Stokes flow · Interfacial flow · Instability · Channel flow

1 Introduction

The study of twin and multi-component fluid systems forms a very large area of research. Applications include fluid mixing, oil recovery from lubricated pipelines, and airflow in the lungs. The effect of wall oscillations on the stability of two-layered flows has received the attention of a number of workers. Most previous studies have focussed on horizontal-wall oscillations, which have either a stabilizing or destabilizing influence, depending on the values of the controlling parameters. Yih (1) considered the stability of a layer of fluid moving on a flat wall executing simple harmonic motion in its own plane. This was extended by von Kerczek (2) to flow down a vertical plate performing a similar motion. Coward and Papageorgiou (3) studied oscillatory Couette flow of two superposed layers in a channel whose upper wall is translating parallel to itself with both a steady and an oscillatory component. Working under the assumption of long waves, they applied Floquet theory to show that a time-dependent modulation can entirely stabilize a

M. G. Blyth (✉)
School of Mathematics, University of East Anglia, Norwich NR4 7TJ, England, UK
e-mail: m.blyth@uea.ac.uk

two-layer Couette flow which is unstable under steady conditions. Halpern and Frenkel (4) considered the nonlinear stability characteristics for the same problem but when the motion of the upper wall is purely oscillatory. The effect of oscillations on core-annular flow has also been studied (e.g., Coward et al. (5), Halpern and Grotberg (6)).

The effect of vertical wall oscillations on interfacial stability appears to have received very little attention. In this article, we investigate the combined and repeated effects of stretching and contracting on a two-layered flow confined between a pair of vibrating walls. Recent work by Pozrikidis and Blyth (7) showed that the presence or absence of a wall in a stretching flow can make an important difference to the stability of superposed fluid layers. When two semi-infinite, unstably stratified fluids are exposed to a straining flow, the gradual increase in the wave length of a disturbance first acts to produce a negative growth rate before the effect of the density stratification takes over and destabilizes the flow. So an extensional flow is unable to suppress the Rayleigh–Taylor instability which occurs for quiescent layers. If the direction of flow is reversed, the wave length of a disturbance tends to contract. An initial period of transient growth is followed by long-term decay as surface tension dominates and stabilizes the flow. Including a lower wall significantly alters the stability; in this case, an elongational flow is able to stabilize interfacial waves.

Our configuration consists of two superposed layers of viscous fluid in a channel whose width changes as a periodic function of time. Each period includes both a stretching and a drawing motion and it is not clear how this will affect the stability of the flow. When the walls move towards each other, the induced squeezing flow produces a stretching effect and small-amplitude disturbances at the interface might naïvely be expected to grow for unstably stratified layers. Similarly, the drawing motion obtained when the walls are pulled apart might be expected to calm interfacial waves. However, the combined effects of both stretching and contracting and the presence of the channel walls are likely to have important consequences for the flow stability which are difficult to predict in advance. We perform a linear stability analysis at zero Reynolds number and use a Floquet method to compute the growth rates of linear waves. At arbitrary Reynolds number, we investigate the flow produced by either a purely squeezing or purely drawing motion, and by the time-periodic pulsation of the channel walls. Working on the assumption that the interface remains flat, we compute the flow under a variety of parametric conditions, and pay particular attention to the trajectory of the interface as the flow evolves.

The layout of the paper is as follows. In Sect. 2, we formulate the linear stability problem for Stokes flow. In Sect. 3, we compute the basic flow numerically for finite Reynolds number on the assumption of a flat interface. Finally, in Sect. 4, we discuss our findings.

2 Channel flow at zero Reynolds number

We consider the motion of two superposed fluid layers in a channel when the walls of the channel move up and down in a prescribed manner so that the channel width is a known function of time. The lower fluid, labelled fluid 1, has density ρ_1 and viscosity μ_1, and the upper fluid, labelled fluid 2, has density ρ_2 and viscosity μ_2. Gravity acts in the vertical direction perpendicular to the channel walls. In the unperturbed configuration, the interface between the layers is assumed to be perfectly flat and parallel to the walls. The walls are located at $y = \pm H(t)$, where $H(t)$ is a specified function of time. The interface is located at the unknown position $y = h(t)$, where $h(t)$ is to be found as part of the solution. The horizontal and vertical velocity components for the unperturbed flow in each fluid, denoted by u_j and v_j respectively for $j = 1, 2$, are given in terms of the unperturbed streamfunctions by the usual relations, $u_j = \partial\psi_j/\partial y$ and $v_j = -\partial\psi_j/\partial x$. Following Hall and Papageorgiou (8), we assume a linear dependence on the horizontal coordinate and write

$$\psi_j = x\, V_j(y,t). \tag{2.1}$$

At zero Reynolds number, the velocity and pressure satisfy the steady Stokes equations of fluid motion. When a flat interface is assumed, the solution in either fluid is given by

$$V_j = \frac{\dot{H}}{H^3\Lambda(t)}\left[\beta_{0j}(t) + \beta_{1j}(t)y + \beta_{2j}(t)y^2 + \beta_{3j}(t)y^3\right] \tag{2.2}$$

for $j = 1, 2$, and

$$\begin{aligned}
\beta_{0j} &= H^3(1-\lambda)[\,(-1)^j(\lambda-1)\,r^4 + 4(-1)^j(1+\lambda)\,r^3 + 6m_{3-j}\,r^2 \\
&\quad +4(\lambda-1)\,r + (1+\lambda)\,], \\
\beta_{1j} &= 12H^2 m_j\left[\,(-1)^{j+1}(1-\lambda)\,r^2 + (1-\lambda)\,r - 2m_{3-j}\,\right], \\
\beta_{2j} &= 6Hm_j(1-\lambda)(r^2-1), \\
\beta_{3j} &= 4m_j\left[\,(\lambda-1)\,r + (1+\lambda)\,\right], \\
\Lambda &= (\lambda-1)^2\,r^2(r^2+6) + 4(\lambda^2-1)\,r(r^2+1) + (1+14\lambda+\lambda^2),
\end{aligned} \tag{2.3}$$

where $r(t) = h(t)/H(t)$ and the viscosity ratio $\lambda = \mu_2/\mu_1$, with the additional definitions $m_1 = \lambda$ and $m_2 = 1$. The solution (2.2) satisfies no-slip and no-penetration at the moving walls,

$$V_1(-H,t) = \dot{H}, \quad \frac{\partial V_1}{\partial y}(-H,t) = 0, \quad V_2(H,t) = -\dot{H}, \quad \frac{\partial V_2}{\partial y}(H,t) = 0, \tag{2.4}$$

together with conditions of continuity of velocity and stress at the flat interface. It can be shown that, at a fixed x-station, the axial velocity field, u_j, is of the same form as that for plane Poiseuille flow of two superposed layers, with the flux in each layer a function of time dependent on $H(t)$.

The pressure fields in the two fluids are given by

$$\begin{aligned}
p_1^{(0)} &= \frac{\mu_1}{2}x^2\frac{\partial^3 V_1}{\partial y^3} - \rho_1 gh - \mu_1\frac{\partial V_1}{\partial y} + P_0, \\
p_2^{(0)} &= \frac{\mu_2}{2}x^2\frac{\partial^3 V_2}{\partial y^3} - \rho_2 gh - \mu_2\frac{\partial V_2}{\partial y} + \frac{24\dot{H}}{H\Lambda}\mu_1\lambda(r^2-1)(\lambda-1) + (\rho_2-\rho_1)gh + P_0,
\end{aligned} \tag{2.5}$$

where P_0 is a reference pressure. The pressure undergoes a jump across the interface given by

$$p_1^{(0)}(y=h) - p_2^{(0)}(y=h) = -\frac{48\dot{H}}{H\Lambda}\mu_1\lambda(r^2-1)(\lambda-1). \tag{2.6}$$

When the viscosities are equal and $\lambda = 1$, Eq. 2.2 reduces to the time-periodic Stokes flow solution given by Hall and Papageorgiou (8) for a single fluid. For general $\lambda \neq 1$, the kinematic condition at the interface yields the evolution equation for the interface position, $h(t)$, given by $\mathrm{d}h/\mathrm{d}t = v(h,t) = -V_1(h,t)$. Equivalently,

$$\frac{\mathrm{d}r}{\mathrm{d}t} = -\frac{\dot{H}}{H\Lambda(t)}\,(\lambda-1)^2(r^2-1)(r-w)(r-1/r^*)(r-r^*), \tag{2.7}$$

where $w = (1+\lambda)/(1-\lambda)$, and

$$r^* = \frac{1-\lambda^{1/2}}{1+\lambda^{1/2}}. \tag{2.8}$$

Evidently, if $r = r^*$, then $\mathrm{d}r/\mathrm{d}t = 0$ for all time and the ratio of the two layer thicknesses, given by

$$\frac{1-r^*}{1+r^*} = \lambda^{1/2} \tag{2.9}$$

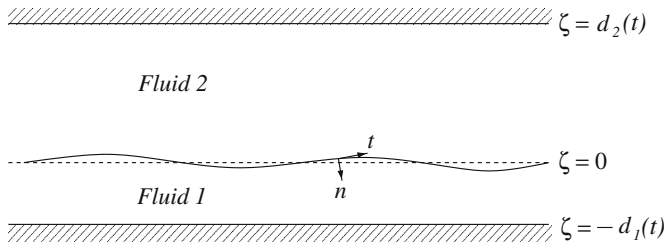

Fig. 1 Sketch of the periodic perturbation to the two-layer flow. The unperturbed interface is at $\zeta = 0$. The unit normal **n** and unit tangent **t** point into the lower fluid and in the direction of increasing arc length, respectively

remains constant throughout the motion. In general, (2.7) is to be integrated subject to a suitable initial condition $r(0) = r_0$. Carrying out the integration, we find

$$\frac{(r - r^*)^2\,(r - 1/r^*)^2}{(r^2 - 1)\,(d - r)^3} = cH(t), \tag{2.10}$$

where c is a constant determined by the initial condition. Evidently, the movement of the interface is synchronous with the wall motion, as was to be expected in the absence of inertia. For an oscillatory flow, with $H(t)$ a periodic function of time, the interface must return to its starting position after one period in accordance with the reversibility of Stokes flow. If $r_0 > r^*$, for example, the interface remains trapped in the region $(r^*, 1)$ throughout the motion.

To investigate the stability of the two-layer channel problem under conditions of Stokes flow, we consider the effect of introducing a spatially periodic disturbance in the interface shape. In the ensuing analysis it is convenient to change to a new frame of reference in which the unperturbed, flat interface is fixed. Accordingly, we introduce the new vertical coordinate, ζ, defined so that $\zeta = y - h(t)$. In the new frame, illustrated in Fig. 1, the unperturbed interface is positioned at $\zeta = 0$, and the upper and lower walls are located at $\zeta = -d_1(t)$ and $\zeta = d_2(t)$ respectively, where

$$d_1 = H + h, \quad d_2 = H - h. \tag{2.11}$$

The interface is deflected to a new position given by$\zeta = f(x,t) = \epsilon\,\eta(x,t)$, where ϵ is a small parameter. To study a spatially periodic deflection, we assume that

$$\eta = A_1(t)\cos[k(t)x], \tag{2.12}$$

where the wave amplitude, $A_1(t)$, and the wave number, $k(t)$, are both functions of time. In response to the perturbation, the stream functions in the two fluids are expanded by writing $\psi_j = \psi_j^{(0)}(x,\zeta,t) + \epsilon\,\psi_j^{(1)}(x,\zeta,t) + \cdots$, where the basic flow is given by

$$\psi_j^{(0)}(x,\zeta,t) = x\left[\,V_j(\zeta,t) + \dot{h}\,\right], \tag{2.13}$$

and V_j is given in (2.2). The vertical fluid velocity at the unperturbed interface, $\zeta = 0$, is zero for the unperturbed flow.

Following Pozrikidis and Blyth (7), we decompose the disturbance stream function in either fluid into a periodic part and a part which is odd in x by writing

$$\psi_j^{(1)}(x,\zeta,t) = A_1\Big[\,\phi_j(\hat{\zeta})\,\sin[k(t)x] + \hat{x}\,\chi_j(\hat{\zeta})\,\cos[k(t)x]\,\Big], \tag{2.14}$$

where $\hat{x} = kx$ and $\hat{\zeta} = k\zeta$. The second, aperiodic term is included to ensure continuity of the horizontal velocity perturbation at the disturbed interface. At zero Reynolds number, the disturbance stream function satisfies the biharmonic equation in each fluid. The general solutions are

$$\phi_j = a_{1j}(t)\mathrm{e}^{\hat{\zeta}} + a_{2j}(t)\hat{\zeta}\mathrm{e}^{\hat{\zeta}} + a_{3j}(t)\mathrm{e}^{-\hat{\zeta}} + a_{4j}(t)\hat{\zeta}\mathrm{e}^{-\hat{\zeta}} + \hat{\phi}_j(\hat{\zeta},t),$$
$$\chi_j = \alpha_{1j}(t)\mathrm{e}^{\hat{\zeta}} + \alpha_{2j}(t)\hat{\zeta}\mathrm{e}^{\hat{\zeta}} + \alpha_{3j}(t)\mathrm{e}^{-\hat{\zeta}} + \alpha_{4j}(t)\hat{\zeta}\mathrm{e}^{-\hat{\zeta}} \tag{2.15}$$

for $j = 1, 2$, where the functions a_{ij}, α_{ij}, $i = 1, \ldots, 4$ are to be found, and

$$\hat{\phi}_j = -\frac{1}{k}\mathrm{e}^{-\hat{\zeta}}\left(\frac{3}{2} + 2\,\hat{\zeta} + \hat{\zeta}^2\right)\alpha_{4j} + \frac{1}{k}\mathrm{e}^{\hat{\zeta}}\left(\frac{3}{2} - 2\,\hat{\zeta} + \hat{\zeta}^2\right)\alpha_{2j}. \tag{2.16}$$

We write the corresponding perturbation pressure fields in the form

$$p_j^{(1)}(x,\zeta,t) = A_1\,\mu_j\left(q_j(\zeta,t)\ \cos[k(t)x] + \hat{x}\,Q_j(\zeta,t)\ \sin[k(t)x]\right) \tag{2.17}$$

for $j = 1, 2$. By substituting (2.17) in the horizontal component of the Stokes equation and integrating, we find

$$q_j = \frac{1}{k}\left[\left(\frac{\mathrm{d}^3\chi_j}{\mathrm{d}\zeta^3} + k^2\frac{\mathrm{d}\chi_j}{\mathrm{d}\zeta}\right) - \left(\frac{\mathrm{d}^3\phi_j}{\mathrm{d}\zeta^3} - k^2\frac{\mathrm{d}\phi_j}{\mathrm{d}\zeta}\right)\right], \quad Q_j = \frac{1}{k}\left(\frac{\mathrm{d}^3\chi_j}{\mathrm{d}\zeta^3} - k^2\frac{\mathrm{d}\chi_j}{\mathrm{d}\zeta}\right). \tag{2.18}$$

The no-slip and no-penetration conditions at the walls require that

$$\phi_j = \chi_j = \frac{\partial\phi_j}{\partial\zeta} = \frac{\partial\chi_j}{\partial\zeta} = 0 \tag{2.19}$$

at $\zeta = -d_1$ for $j = 1$ and $\zeta = d_2$ for $j = 2$. These conditions yield 8 relations between the 16 unknown functions a_{ij}, α_{ij}, $i = 0, \ldots, 3$. The horizontal interfacial force balance requires

$$\left[2\mu_j\frac{\partial\eta}{\partial x}\left(\frac{\partial u_j^{(0)}}{\partial x} - \frac{\partial v_j^{(0)}}{\partial\zeta}\right) - \mu_j\left(\frac{\partial u_j^{(1)}}{\partial\zeta} + \frac{\partial v_j^{(1)}}{\partial x} + \eta\frac{\partial^2 u_j^{(0)}}{\partial\zeta^2}\right)\right]_2^1 = 0, \tag{2.20}$$

where $[\cdot]_2^1 = [\cdot]_1 - [\cdot]_2$. Substitution in the preceding expressions yields two relations between the unknown coefficients. Denoting the surface tension by γ_0, the vertical interfacial force balance requires

$$p_2^{(1)} - p_1^{(1)} + 2\mu_1\frac{\partial v_1^{(1)}}{\partial\zeta} - 2\mu_2\frac{\partial v_2^{(1)}}{\partial\zeta} + (1-\delta)\rho_1 g\eta = \gamma_0\frac{\partial^2\eta}{\partial x^2}, \tag{2.21}$$

where $\delta = \rho_2/\rho_1$ is the density ratio, g is the acceleration due to gravity, and all terms evaluated at the unperturbed interface $\zeta = 0$. Substituting in the preceding expressions, we derive two further relations between the unknown coefficients. Continuity of the horizontal and vertical velocities at the interface demands

$$u_1^{(1)} + \eta\frac{\partial u_0^{(1)}}{\partial\zeta} = u_1^{(2)} + \eta\frac{\partial u_0^{(2)}}{\partial\zeta}, \quad v_1^{(1)} + \eta\frac{\partial v_0^{(1)}}{\partial\zeta} = v_1^{(2)} + \eta\frac{\partial v_0^{(2)}}{\partial\zeta}, \tag{2.22}$$

where all terms are evaluated at $\zeta = 0$. These relations provide a further four conditions on the unknowns. We now have available 16 conditions for the 16 unknowns, which we compile into the matrix system

$$\mathbf{M}(\mathrm{t})\cdot\mathbf{w} = \mathbf{b}(\mathrm{t}), \tag{2.23}$$

where $\mathbf{M}$ is a known 16×16 matrix, the solution vector $\mathbf{w} = (a_{11}, \ldots, \alpha_{42})^{\mathrm{T}}$, containing all of the unknown coefficients, and $\mathbf{b}$ is the vector of inhomogeneous terms. It will be noted that Eq. 2.23 is independent of A_1.

The kinematic condition at the interface requires that

$$\frac{\partial\eta}{\partial t} + u_1^{(0)}\frac{\partial\eta}{\partial x} - \eta\frac{\partial v_1^{(0)}}{\partial\zeta} - v_1^{(1)} = 0 \tag{2.24}$$

with all terms evaluated at $\zeta = 0$. Applying the previous results in (2.24), we derive the evolution equation for the wave number,

$$\frac{\mathrm{d}k}{\mathrm{d}t} + \frac{24\dot{H}}{H\Lambda(t)}\lambda(r^2-1)\,k + [\alpha_{11}+\alpha_{31}]\,k^2 = 0, \tag{2.25}$$

and the evolution equation for the interfacial perturbation amplitude,

$$\frac{\mathrm{d}A_1}{\mathrm{d}t} + \mathcal{L}(t)A_1 = 0 \tag{2.26}$$

with

$$\mathcal{L}(t) = \frac{24\dot{H}}{H\Lambda(t)}\lambda(r^2-1) + k(\alpha_{11}+\alpha_{31}+a_{11}+a_{31}) + \frac{3}{2}(\alpha_{21}-\alpha_{41}), \tag{2.27}$$

where $r = h/H = (d_2-d_1)/(d_2+d_1)$ and Λ is given in (2.3). The coefficients $\alpha_{11}, \alpha_{31}, a_{11}$ and a_{31} are functions of k but are independent of A_1. Thus, the evolution equation for k is decoupled from the evolution equation for A_1.

To provide a check on the above formulation, we consider the case of equal-density fluids confined between stationary walls and set $\dot{H} \equiv 0$ for all t. According to Yih (9), a flat interface between two quiescent layers in a channel is stable at zero Reynolds number. Blyth and Pozrikidis (10) showed that the growth rate of a small perturbation in a two-layered channel flow is independent of the structure of the basic flow, and depends solely on the local shear rates just above and below the interface. Solving the linear system (2.23), we find that all but the first term in (2.26) vanishes, implying a constant wave number. The first equation in (2.23) reduces to $\mathrm{d}A_1/\mathrm{d}t + \sigma A_1 = 0$, where the growth rate $\sigma = k(a_{11}+a_{31})$. Substituting the known values of a_{11} and a_{31}, we obtain perfect agreement with the results of Blyth and Pozrikidis (10).

To focus on the case when H is a periodic function of time, throughout the remainder of this section we take

$$H(t) = H_0(1+\Delta\cos nt), \tag{2.28}$$

where H_0, n, and Δ are real constants, with $0 < \Delta < 1$. We assume that the timescale of the pulsations is sufficiently large compared with the viscous diffusion time, $1/n \gg H_0^2/\nu$, to justify the omission of the unsteady term in the Stokes equations. Defining a Reynolds number based on the pulsation frequency,

$$R = \frac{\rho n H_0^2}{\mu_1}, \tag{2.29}$$

this is equivalent to assuming that $R \ll 1$. Under this assumption, the basic flow is described by (2.2) and is periodic in time with period $T = 2\pi/n$. According to Floquet theory (e.g. (11, Chapter 5.4)), a small perturbation from a time-periodic solution may be expressed as the product of an exponentially growing part and a time-periodic part. Given the form of (2.14), we may therefore write

$$A_1 = \mathrm{e}^{st}A(t) \tag{2.30}$$

for constant s, where $A(t)$ is a periodic function of time such that $A(t+T) = A(t)$. Consequently, the coefficients $a_{ij}(t), \alpha_{ij}(t)$, for $i = 1,\ldots 4$ and $j = 1,2$, are all periodic with period T. It follows from the linear system (2.23) that the wave-number $k(t)$ must also be periodic with period T. Therefore the solution to the wave-number evolution equation (2.25) must also turn out to be periodic in time with the same period. This has been confirmed numerically. The stability is determined by calculating the Floquet exponent s: If $s > 0$, the flow is unstable, and if $s < 0$, the flow is stable. Dimensional analysis shows that the stability characteristics are governed by the viscosity ratio λ, the density ratio δ, and the capillary and Bond numbers defined by

$$\mathrm{Ca} = \frac{\mu_1 H_0 n}{\gamma_0}, \quad \mathrm{Bo} = \frac{H_0^2|\rho_1-\rho_2|g}{\gamma_0}. \tag{2.31}$$

To assess the stability of the system for different parameter values, we integrate equations (2.25) and (2.26) forward in time numerically using second order Runge–Kutta integration. At each part of the integration step, the linear system (2.23) is solved to find **w**. To compute the Floquet exponent, the equations are integrated from $t = 0$ over a period of length T. From (2.30),

$$s = \frac{1}{T}\log\left\{\frac{A_1(T)}{A_1(0)}\right\} = -\frac{1}{T}\int_0^T \mathcal{L}(t)\mathrm{d}t. \tag{2.32}$$

Since $\mathcal{L}(t)$ is periodic with period T, it follows that the Floquet exponent is independent of the frequency of the pulsations, n. To provide a check on the calculation of the Floquet exponent, we consider the case of equal-density fluids, $\delta = 1$, and confirm that the transformation $\lambda \to 1/\lambda$, $r_0 \to -r_0$, which corresponds to turning the channel upside-down, does not affect the computed value of the growth rate.

When the fluids have the same density, the interface is stable under all conditions. However, the pulsations tend to lower the decay rate of linear perturbations, and in this sense they are destabilizing. The dimensionless growth rate $s^* \equiv (\mu_1 H_0/\gamma_0)s$, where $H_0 = H(0)$, is shown in Fig. 2 for the sample case $\delta = 1$, $\lambda = 0.5$, $r_0 = 0.5$ and $\mathrm{Ca} = 2.0$. Results are plotted over a range of reduced initial wave numbers k_0H_0, where $k_0 = k(0)$, for a number of different wall amplitudes. The growth rates increase as the wall amplitude increases, and so the pulsations have a destabilizing influence on the flow. The effect of varying the viscosity stratification is shown in Fig. 2(b). Increasing λ lowers the decay rate of perturbations and in this sense has a destabilizing effect. To assess the effect of the wall pulsations on the Rayleigh–Taylor instability, in Fig. 3(a) we plot s^* against k_0H_0 for the case $\delta = 1.5$, $\lambda = 0.5$, $r_0 = 0$, $\mathrm{Ca} = 2.0$ and $\mathrm{Bo} = 0.5$. In this figure, the unperturbed interface lies midway between the walls at $t = 0$, so that r_0 is zero. The heavier fluid lies on top of the lighter fluid yielding instability over a range of wave numbers between zero and the critical cut-off value k_c. For smaller wave numbers, the pulsations lower the growth rate of small disturbances and so promote the stability of the flow. For larger wave numbers close to the cut-off value, the pulsations increase the growth rate thereby promoting the instability. The dependence of the critical wave number k_c on the amplitude of the vibrations is shown in Fig. 3(b). Initially, it increases from its value for a static channel, with $\Delta = 0$, before reaching a peak at $\Delta \approx 0.23$. Thus, the effect of the pulsations is to extend the range of unstable wave numbers.

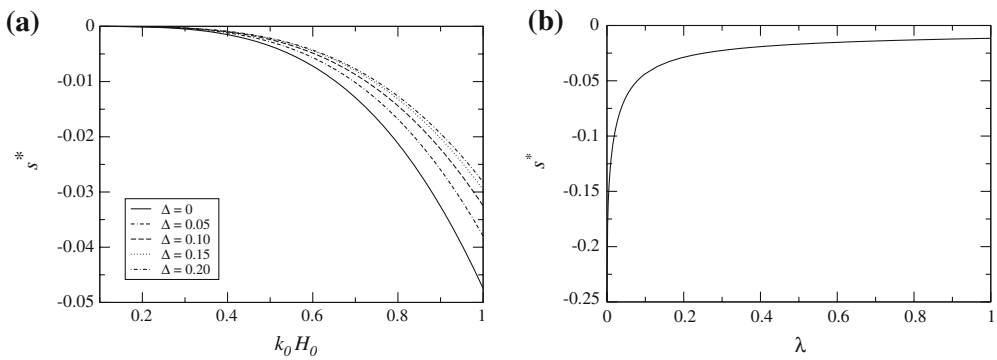

Fig. 2 Dimensionless growth rate s^* for equal density fluids, $\delta = 1$ and $\mathrm{Ca} = 2.0$: (**a**) s^* versus reduced initial wave number k_0H_0 when $\lambda = 0.5$, $r_0 = 0$ for various Δ; (**b**) s^* versus viscosity ratio λ for $r_0 = 0.5$, $\Delta = 0.1$ and $k_0H_0 = 1.0$

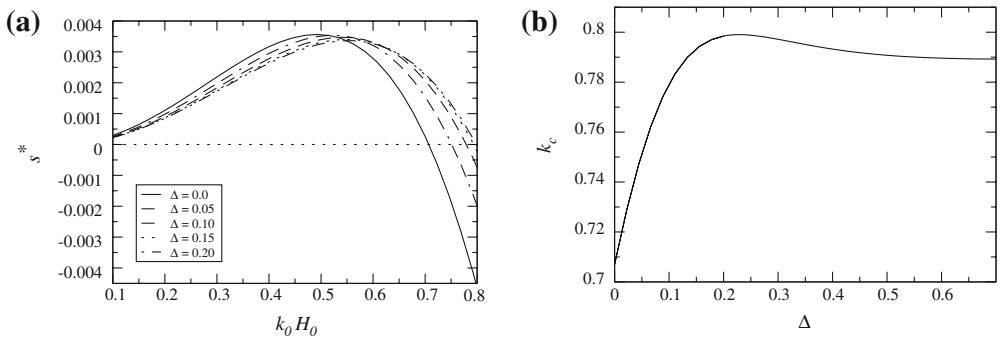

Fig. 3 The case $\delta = 1.5$, $\lambda = 0.5$, $r_0 = 0$, Ca $= 2.0$ and Bo $= 0.5$: (**a**) Floquet exponent s^* against reduced initial wave number k_0H_0 for a range of wall amplitudes, Δ. (**b**) Variation of critical wave number k_c with wall amplitude Δ

3 Channel flow at arbitrary Reynolds number

In this section we consider the two-fluid channel-flow problem for general Reynolds number. The fluids are assumed to be of equal density, ρ, and the interface is assumed to be flat and to remain parallel to the walls at all times. As in Sect. 2.1, the flow domain is $-H(t) \le y \le H(t)$, where $H(t)$ is a prescribed function of time and the flat interface is located at $y = h(t)$.

We seek a solution of stagnation-point form in which the horizontal velocity depends linearly on the horizontal coordinate. Specifically, we take

$$\psi_j = xV_j(y,t) \tag{3.1}$$

for $j = 1, 2$. Using $1/n$ as a reference time scale and the mean channel thickness H_0 as the reference length, we nondimensionalize by writing $t = nt^*$, $(x, y) = H_0(x^*, y^*)$, $H = H_0H^*$, and $\psi_j = (nH_0^2)\,\psi_j^*$, where asterisks indicate dimensionless variables. We map the flow field onto the fixed domain $[-1, 1]$ by introducing the new coordinate $\eta = y/H(t)$. When the asterisks are dropped for convenience, the Navier–Stokes equation yields the following system for the flow in each fluid,

$$\frac{\partial^3 V_j}{\partial\eta^2\partial t} = \frac{\dot H}{H}\left(2\frac{\partial^2 V_j}{\partial\eta^2} + \eta\frac{\partial^3 V_j}{\partial\eta^3}\right) + \frac{1}{H}\left(V_j\frac{\partial^3 V_j}{\partial\eta^3} - \frac{\partial V_j}{\partial\eta}\frac{\partial^2 V_j}{\partial\eta^2}\right) + \frac{m_j}{H^2R}\,\frac{\partial^4 V_j}{\partial\eta^4}, \tag{3.2}$$

where $j = 1, 2$, $m_1 = 1$ and $m_2 = \lambda = \mu_2/\mu_1$. The Reynolds number R was defined in (2.29). Taking the limit $R \to 0$ reduces the problem to that studied in Sect. 2. The boundary conditions on (3.2) are no-slip and no-penetration at the walls, (2.4), together with continuity of velocity at the interface,

$$V_1 = V_2, \quad \frac{\partial V_1}{\partial\eta} = \frac{\partial V_2}{\partial\eta} \tag{3.3}$$

at $\eta = r(t)$, where $r(t) = h(t)/H(t)$. Continuity of tangential stress at the interface requires that

$$\frac{\partial^2 V_1}{\partial\eta^2} = \lambda\frac{\partial^2 V_2}{\partial\eta^2} \tag{3.4}$$

at $\eta = r(t)$. The solution for Stokes flow, valid at $R = 0$, is given by (2.2). The dimensionless kinematic condition at the interface leads to the obvious evolution equation for the interfacial position $h = rH$,

$$\frac{\mathrm{d}}{\mathrm{d}t}(rH) = -V_1(r,t). \tag{3.5}$$

Finally, if we integrate (3.2) across the moving interface from $\eta = r_-(t)$ up to $\eta = r_+(t)$, taking care to account for the time-dependent limits, and make use of (3.5) to simplify, we obtain the jump condition

$$\frac{\partial^3 V_1}{\partial \eta^3} = \lambda \frac{\partial^3 V_2}{\partial \eta^3} \tag{3.6}$$

at $\eta = r(t)$.

In the following subsection, we discuss periodic solutions for small values of Δ. Thereafter, we introduce the numerical method to solve the system for arbitrary values of R and Δ, and present some results.

3.1 Small-amplitude periodic solution

At zero Reynolds number, we showed in Sect. 2 that the flow is time-periodic with the same period as the wall motion. When inertia is present, we do not in general expect the interfacial trajectory to follow a periodic cycle. For a specific value of r, however, we might expect to be able to find a solution where the layer thickness ratio remains constant throughout the motion, and the flow is periodic in time. For Stokes flow, this occurs when $r = r^*$, where r^* is given by (2.8). To check this possibility at finite Reynolds number, we seek a periodic solution with r constant. To simplify the analysis, we make the further assumption that the amplitude of the wall oscillations is small, so $\Delta \ll 1$.

First, we make the transformation $V_j = -\eta \dot{H} + H^3 \psi_j$, for $j = 1, 2$, and substitute in (3.2) to obtain

$$\frac{\partial^3 \psi_j}{\partial \eta^2 \partial t} = H^2 \left(\psi_j \frac{\partial^3 \psi_j}{\partial \eta^3} - \frac{\partial \psi_j}{\partial \eta} \frac{\partial^2 \psi_j}{\partial \eta^2} \right) + \frac{\lambda_j}{H^2 R} \frac{\partial^4 \psi_j}{\partial \eta^4} \tag{3.7}$$

with the boundary conditions

$$\psi_1(-1, t) = 0, \quad \frac{\partial \psi_1}{\partial \eta}(-1, t) = \frac{\dot{H}}{H^3}, \quad \psi_2(1, t) = 0, \quad \frac{\partial \psi_2}{\partial \eta}(1, t) = \frac{\dot{H}}{H^3}. \tag{3.8}$$

The conditions on ψ_j at the interface are identical to (3.3), (3.4) and (3.6). Assuming that r is constant, we observe that the kinematic condition (3.5) requires

$$\psi_j(r, t) = 0. \tag{3.9}$$

To obtain the solution for small Δ, we expand in either fluid by writing

$$\psi_j(\eta, t) = \Delta \, \mathrm{e}^{2\mathrm{i}t} \psi_j^{(0)}(\eta) + \Delta^2 \left[\mathrm{e}^{4\mathrm{i}t} \psi_j^{(1)}(\eta) + \psi_j^{(1s)}(\eta) \right] + \cdots . \tag{3.10}$$

The steady component $\psi_j^{(1s)}$ at first order is driven by the nonlinear terms on the right-hand side of (3.7). Substituting in (3.7) and (3.8), we may write down a sequence of linear problems at successive orders to solve for $\psi_j^{(0)}$ and so on. At leading order, we find that it is possible to find a solution satisfying the wall boundary conditions (3.8), and the interfacial conditions (3.3), (3.4) and (3.6). However, it is only possible to satisfy (3.9) if $r = r^*$, where r^* is given by (2.8) and which depends solely on the viscosity ratio of the two fluids. Thus the periodic Stokes solution (2.2) with $r = r^*$ extends to finite Reynolds numbers for small wall amplitudes. In Sect. 3.3, we show numerically that periodic solutions also exist for arbitrary values of Δ.

3.2 Numerical method for arbitrary wall amplitude

In this section, we describe the numerical method used to compute solutions for any wall amplitude at arbitrary Reynolds number. It will be convenient to transform to a new coordinate system in which the position of the interface is fixed in time. To this end, we introduce the time-dependent piecewise-linear mapping

$$\eta = r + (1 \pm r)\zeta, \tag{3.11}$$

where the plus sign applies for $\eta < r(t)$ and the minus sign applies for $\eta > r(t)$. In the transformed ζ-space, the channel walls are located at $\zeta = \pm 1$, and the interface is located at $\zeta = 0$.

The numerical method is based on the Crank–Nicolson scheme. Although it is similar to that employed by Hall and Papageorgiou (8) for a single fluid, the complications of including a moving interface merit a careful description here. A uniform grid is used in the transformed space with mesh points at $\zeta_i = -1+(i-1)\delta\zeta$, for $i = 1, \ldots 2N+1$, where $\delta\zeta = 1/N$ is the step length. The solution at grid point ζ_i at time level t_n is denoted by $V^n_{j,i}$ in fluid $j = 1, 2$. To advance forward one time step, δt, a discretized form of the momentum equation (3.2) is applied at all of the interior points excluding the interfacial point $i = N + 1$. We approximate the spatial derivatives using centred differences. The linear terms in (3.2) are centered about the mid-point $t_n + \frac{1}{2}\delta t$ in the usual way for Crank–Nicolson integration. Since the coefficient of the time-derivative term in the transformed form of (3.2) is time-dependent, it must be evaluated at $t + \frac{1}{2}\delta t$ to preserve the second-order temporal accuracy of the scheme. At the preliminary stage, the nonlinear terms are treated explicitly at the previous time step, t_n. The first of the matching conditions (3.3) implies that $V^n_{1,N+1} = V^n_{2,N+1}$. Introducing the fictitious points $V^n_{1,N+2}$ and $V^n_{2,0}$, we derive two further conditions by approximating the second equation of (3.3) and (3.4), using centred differences about the interfacial point ζ_{N+1}. These are solved simultaneously to eliminate the two fictitious points. The Neumann boundary conditions at the two walls are dealt with in a similar way.

Combining the discretized momentum equations and boundary conditions, we form the matrix system,

$$\mathbf{A} \cdot \mathbf{V}^{n+1} = \mathbf{B} \cdot \mathbf{V}^n + \mathbf{N}, \tag{3.12}$$

where $\mathbf{V}^n = (V^n_{1,2}, \ldots, V^n_{1,N}, V^n_{2,N+2}, \ldots, V^n_{2,2N})^{\mathrm{T}}$, excluding the unknown interfacial value $V^n_{1,N+1}$. The $(2N-2) \times (2N-2)$ pentadiagonal matrices $\mathbf{A}$ and $\mathbf{B}$ involve knowledge of the unknown value $h_{n+1} \equiv r(t_{n+1})H(t_{n+1})$ and the known value h_n. The vector $\mathbf{N}$ incorporates the nonlinear terms evaluated at the current time step t_n. The matrix system (3.12) is to be solved simultaneously with the discretized form of the evolution equation (3.5),

$$h_{n+1} = h_n - \tfrac{1}{2}\delta t \left(V^{n+1}_{1,N+1} + V^n_{1,N+1} \right). \tag{3.13}$$

To advance to the next time step, t_{n+1}, we first guess the unknown interfacial value $V^{n+1}_{1,N+1}$. Next, we solve (3.12) and (3.13) simultaneously using a modified form of the Thomas algorithm suitable for pentadiagonal systems (e.g., (12, Chapter 3)). To preserve the second-order spatial and temporal accuracy of the scheme, we centre the nonlinear terms at the mid-point $t_n + \frac{1}{2}\delta t$ and iterate in the manner described by Hall and Papageorgiou (8). Typically, only one or two iterations are required to achieve an acceptable level of convergence. The process is repeated and the initial guess for $V^{n+1}_{1,N+1}$ is refined using Newton's method until the jump condition (3.6) is satisfied to within a prescribed tolerance.

The numerical method was checked in a variety of different ways. First, we recomputed results for a single fluid using the method described by Hall and Papageorgiou (8), and compared with the results produced by the present code with $\lambda = 1$. In Fig. 4(a), we show the trajectory, $r(t)$, plotted against time when the forcing function $H(t) = 1 + 0.25\cos 2t$. Throughout the rest of the paper, unless otherwise stated, computations were performed with $N = 120$ grid points in each fluid with a time step $\delta t = 0.001$. Higher-resolution calculations confirmed the accuracy of the results shown. Further checks were carried out under the same conditions by computing the lower-wall shear for two different choices of interfacial starting position, r_0. In the case of equal fluid viscosities, the lower-wall shear is independent of the choice of r_0, and this was verified during a number of simulations. For two fluids, a check on the method was performed at small Reynolds number to compare with the Stokes flow results of Sect. 2. Figure 4(b) shows the interfacial trajectory for the case $\lambda = 0.5$ and $R = 0.1$ with the forcing function $H(t) = 1 + 0.25\cos 2t$.

As an additional check, we confirmed that the results are unchanged under the transformation λ to $1/\lambda$ and r_0 to $-r_0$, which effectively corresponds to turning the channel upside down.

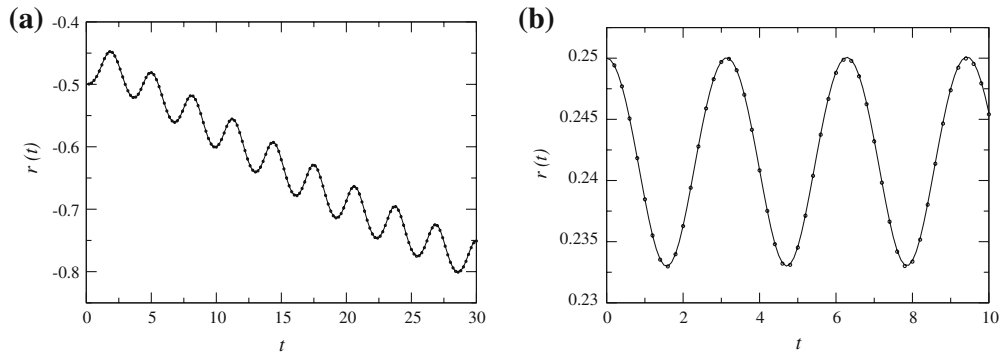

Fig. 4 The interface position $r(t)$ for wall forcing $H(t) = 1 + 0.25\cos 2t$. (**a**) For a single fluid, $\lambda = 1$, with $R = 20$. The solid line is the present result, and the circles represent the result computed using Hall and Papageorgiou's method. (**b**) For two fluids with $\lambda = 0.5$. The solid line shows the result for $R = 0.01$ and the circles show the result for Stokes flow

3.3 Results

To present our results for two superposed fluid layers, we begin by considering squeezing or drawing flow, during which the channel walls are continuously drawn apart or squeezed together. For this purpose, we choose $H(t) = 1 - \sigma t$, where $\sigma = 1$ for squeezing flow and $\sigma = -1$ for drawing flow. Naturally, when $\sigma = 1$, calculations are only valid for $t < 1$. For equal viscosity fluids, if $r_0 = 0$ the interface does not move from the channel centre line during the motion. For two superposed layers, the results depend on the starting position of the interface, as is illustrated in Fig. 5 for the representative case $\lambda = 0.5$ and $R = 20$. Here and below, calculations were started at $t = 0$ from rest with $V_j \equiv 0$ everywhere. When $r_0 = 0$, the interface is pulled upwards towards the less viscous fluid during squeezing motion, and pushed downwards towards the more viscous fluid during drawing motion, as shown by the upper two lines in Fig. 5. The reverse applies when $r_0 = 0.5$, as is demonstrated by the lower two lines in Fig. 5. Now the interface is forced down toward the more viscous fluid under the squeezing motion but lifted up toward the less viscous fluid during the drawing motion. Similar observations are made at other Reynolds numbers. These results suggest that we may be able to select an initial value, r_0, such that $r(t)$ remains constant throughout the subsequent flow. At zero Reynolds number, the appropriate choice is $r = r^*$, where r^* is given by (2.8). Taking $r_0 = r^*$ in a squeezing flow with $\lambda = 0.5$ and $R = 20$ as above, we obtain the result shown in Fig. 5 as a thick solid line. Evidently, r is constant throughout the motion.

We now turn our attention to the case when the wall motion is time-periodic. We take $H(t) = 1 + \Delta\cos t$, with $0 < \Delta < 1$, in which case the flow experiences both a drawing and a squeezing motion during each cycle. We begin by demonstrating that we may compute periodic solutions for small Δ consistent with the analysis of Sect. 3.1. In Fig. 6(a), we show the profile of ψ_j across the channel at the time $t = 10$ for the case $\lambda = 0.5$, $R = 10$ and $\Delta = 0.01$. The interface is situated where the curves cross the axis at $\eta = r^* = 0.172$. The solid line shows the result of the numerical simulation, and the broken line shows the leading-order solution $\Delta\psi_j^{(0)}$ in (3.10). At the time shown, the numerical solution has settled into a periodic cycle, and the profile agrees well with that obtained from the small-amplitude analysis. Periodic solutions also exist at larger values of the wall amplitude, as is discussed below.

In Fig. 6(b), interfacial trajectories are shown for the case $\lambda = 0.5$, $\Delta = 0.25$ and $R = 20.0$ for a number of different starting positions. Evidently, the long-term behaviour of the interface depends upon its initial position. If $r_0 = r^*$, the flow locks onto a periodic cycle and we find that $r = r^*$ throughout the motion. If $r_0 > r^*$ or $r_0 < r^*$, the interface tends to move on average towards the upper or the lower wall, respectively, and eventually the calculation breaks down. The closer the starting position to r^*, the longer the interface

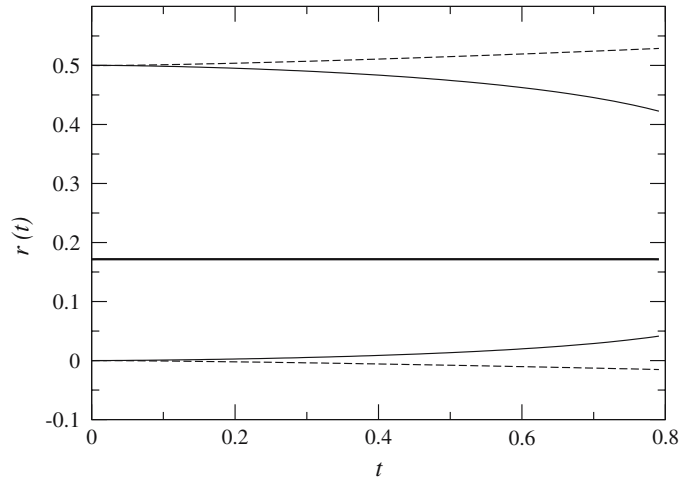

Fig. 5 Squeezing flow (solid line) and drawing flow (broken line) flow at $\lambda = 0.5$, $R = 20$, and for $r_0 = 0$, and $r_0 = 0.5$. The thick solid line shows squeezing flow with $r_0 = r^* = 0.172$

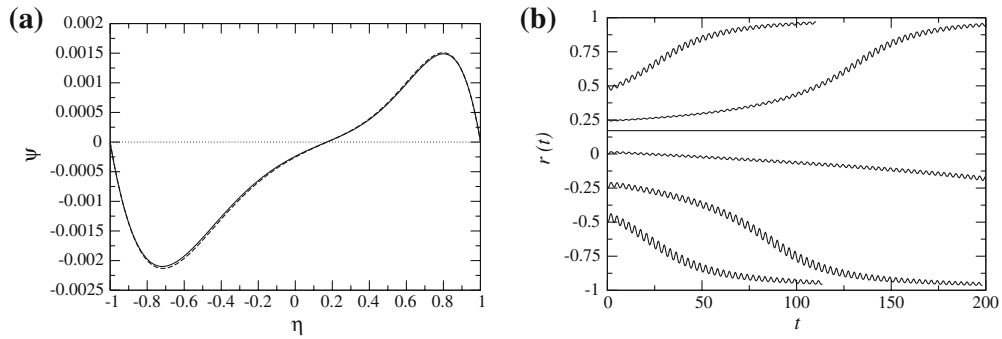

Fig. 6 (**a**) Comparison of the flow profile for the small-amplitude periodic solution (broken line) with the numerical solution with $\Delta = 0.01$ (solid line) for the case $\lambda = 0.5$ and $R = 10$. (**b**) Interfacial trajectories, $r(t)$, for periodic wall motion with $\lambda = 0.5$, $\Delta = 0.25$ and $R = 20$ and starting positions $r_0 = -0.5, -0.25, 0, r^*, 0.25, 0.5$

takes to migrate towards the wall. It seems that all initial positions $r \neq r^*$ eventually approach either of the two walls. The same qualitative behaviour is found on increasing the wall amplitude, but the time taken to approach either the upper or lower wall is reduced. The situation changes when the Reynolds number is increased, as can be seen in Fig. 7(a), which shows results for $\lambda = 0.5$, $\Delta = 0.25$ and $R = 40.0$ for a number of different starting positions. Clearly, there is a catchment area inside which the interface will tend to migrate towards the periodic state at $r = r^*$. Outside of this region, the interface tends towards the upper or lower wall, as is demonstrated by the curves for $r_0 = -0.75$ and $r_0 = 0.75$. Note that for all results shown the interface remains trapped either in the region $(-1, r^*)$ or in the region $(r^*, 1)$. This need not always be the case, as will be demonstrated below at larger wall amplitude.

The effect of varying the viscosity ratio for a flow with $R = 40$ and $\Delta = 0.25$ is shown in Fig. 7(b). In each case, the interface moves towards the respective value of r^*, and the flow tends to approach a periodic state. Trajectories for different wall amplitudes are illustrated in Fig. 8(a) for the case $\lambda = 0.5$ and $R = 40$. All calculations in this figure were started with $r_0 = 0.5$. The curves for $\Delta = 0.1, 0.2, 0.3$ approach the periodic state with $r = r^* = 0.172$ as the time increases beyond that shown in the figure. The smaller the value of Δ, the more slowly the periodic state is approached. Evidently, the long-term behaviour of the interface can depend markedly on the value of Δ. For $\Delta < 0.371$, the interface tends to move downwards

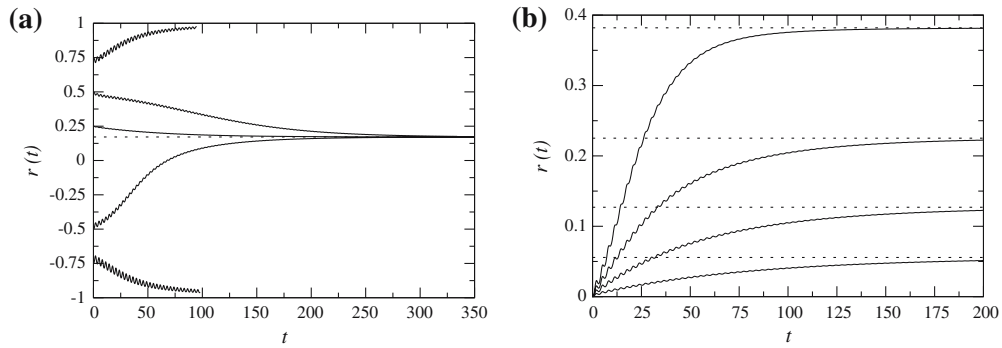

Fig. 7 (**a**) Interfacial trajectories, $r(t)$, against time for $\lambda = 0.5$, $R = 40.0$ and $\Delta = 0.25$ for $r_0 = -0.75$, $r_0 = -0.5$, $r_0 = 0.25$, $r_0 = 0.5$, and $r_0 = 0.75$. The dotted line corresponds to $r^* = 0.172$. (**b**) $\Delta = 0.25$, $R = 40$ and $\lambda = 0.2,\ 0.4,\ 0.6,\ 0.8$, shown as solid lines, where the respective values of $r^* = 0.382,\ 0.225,\ 0.127,\ 0.056$ are shown as dotted lines

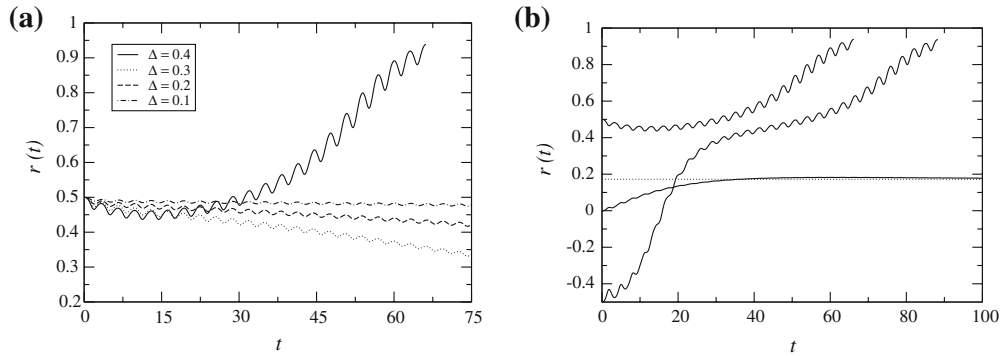

Fig. 8 Interfacial trajectory $r(t)$ against time. (**a**) $\lambda = 0.5$, $R = 40$ and different values of Δ; (**b**) $\lambda = 0.5$, $R = 40$, $\Delta = 0.4$ and $r_0 = -0.5,\ 0,\ 0.5$

towards $r = r^*$. For $\Delta > 0.371$, it moves upwards towards the upper wall. To demonstrate the sensitivity of the trajectory to the starting position in the flow field, we replot the curve for $\Delta = 0.4$ in Fig. 8(b) toegther with the results of the two further starting positions $r_0 = -0.5$ and $r_0 = 0$. The latter curves were computed using $N = 240$ grid points in each fluid with a time step of $\delta t = 0.0005$. The dotted line indicates the position of $r^* = 0.172$. In all calculations shown thus far, the interface has remained trapped in the region $(-1, r^*)$ or $(r^*, 1)$ depending on the starting position. At this higher value of Δ, the interface can cross from one region to the other, as is illustrated by the curve for $r_0 = -0.5$. The trajectory starting with $r_0 = 0$ also crosses the dotted line. It slightly overshoots $r = r^*$ before turning back and slowly approaching the dotted line from above.

4 Concluding remarks

We have examined the flow of two superposed viscous layers in a channel when the motion is induced either by the gradual squeezing together or drawing apart of the walls, or by the vertical vibration of the walls. In the first part, we presented the solution for two-layer Stokes flow in an explicit form and described the motion of the interface. For a particular choice of initial position, the layer thickness ratio remains constant regardless of the motion of the walls. We then considered the stability of the flow at zero Reynolds number by subjecting the interface to a small-amplitude spatially periodic perturbation. The accompanying velocity

field is not spatially periodic, but consists of a periodic part and a component which grows downstream. A Floquet analysis was used to compute the growth rates of the developing disturbance.

Earlier work by Pozrikidis and Blyth (7) showed that a stretching flow is unable to suppress the Rayleigh–Taylor instability present for unstably stratified semi-infinite fluid layers at zero Reynolds number. However, if a bottom wall is included to bound the lower fluid, an elongational flow is able to ultimately suppress periodic disturbances. In the present work, two parallel walls vibrate to produce an alternately stretching and contracting flow. Working in concert, these effects are not able to suppress the Rayleigh–Taylor instability. Rather they tend to increase the growth rate of small disturbances and extend the range of unstable wave numbers, which grows as the amplitude of the wall vibrations is increased. The pulsations therefore have a destabilizing effect on the flow field. Even so, vertical wall oscillations are not sufficient on their own to destabilize a stably stratified flow.

In the second part of the paper, we have computed the basic flow of two superposed fluids in a vibrating channel at arbitrary Reynolds number under the assumption that the interface stays perfectly flat throughout the motion. We used a numerical method to determine the trajectory of the interface. The flow was started from rest and, in the first instance, the walls were either drawn apart or squeezed together continuously. For an initially symmetric configuration with equal layer thicknesses, the interface tends to migrate toward the less viscous fluid when the channel squeezes shut, and toward the more viscous fluid as the channel walls are drawn apart. The opposite behaviour applies if, in the initial configuration, the more viscous layer is thicker than the less viscous layer. For a judicious choice of starting position, the ratio of the layer thicknesses stays constant during the drawing or squeezing motion.

The behaviour of the interface was also investigated when the walls vibrate up and down periodically in time. The subsequent behaviour of the interface depends on its starting position in the flow field, and the prevailing parameter values. At low Reynolds number, the interface tends to approach one of the two walls. At higher Reynolds number, the interface tends to be attracted towards the position where the layer thickness ratio remains constant and the flow becomes time-periodic. This position is solely dependent on the viscosity ratio of the two fluids. As the wall amplitude is increased, the subsequent interfacial trajectory becomes increasingly sensitive to its initial position in the flowfield. For some initial conditions, the flow may approach the time-periodic state, and for others the interface may cross the time-periodic position and head towards one of the channel walls.

The important question of the stability of the interface at finite Reynolds number has not been addressed. Unfortunately, the same approach applied for studying the stability of Stokes flow is frustrated at finite Reynolds number by the nonlinear inertia terms. Despite this, analytical progress may be possible via a lubrication-type analysis, and this will form the subject of a future investigation.

Acknowledgments This research was supported by the Nuffield Foundation under grant NUF-NAL-O4.

References

1. Yih CS (1968) Instability of unsteady flows or configurations Part 1. Instability of a horizontal liquid layer on an oscillating plane. J Fluid Mech 31:737–751
2. von Kerczek CH (1987) Stability characteristics of some oscillatory flows – Poiseuille, Ekman and films. In: Dwoyer DL, Hussaini MY (eds) Stability of time dependent and spatially varying flows. Springer, Berlin
3. Coward AV, Papageorgiou DT (1994) Stability of oscillatory two-phase Couette flow. IMA J Appl Math 54:75–93
4. Halpern D, Frenkel AL (2001) Saturated Rayleigh–Taylor instability of an oscillating Couette film flow. J Fluid Mech 446:67–93
5. Coward AV, Papageorgiou DT, Smyrlis YS (1995) Nonlinear stability of oscillatory core-annular flow: A generalized Kuramoto–Sivashinsky equation with time periodic coefficients. Z angew Math Phys 46:1–39
6. Halpern D, Grotberg JB (2003) Nonlinear saturation of the Rayleigh instability due to oscillatory flow in a liquid-lined tube. J Fluid Mech 492:251–270

7. Pozrikidis C, Blyth MG (2004) Effect of stretching on interfacial stability. Acta Mechanica A 170:149–162
8. Hall P, Papageorgiou DT (1999) The onset of chaos in a class of Navier–Stokes solutions. J Fluid Mech 393:59–87
9. Yih CS (1967) Instability due to viscosity stratification. J Fluid Mech 27:337–352
10. Blyth MG, Pozrikidis C (2004) Effect of surfactants on the stability of two-layer channel flow. J Fluid Mech 505:59–86
11. Drazin PG (1992) Nonlinear systems. Cambridge University Press, Cambridge
12. Pozrikidis C (1998) Numerical computation in science and engineering. Oxford University Press, Oxford